Influence of lubricious oxides formation on the tribological behavior of Mo-V-Cu-N coatings deposited by HIPIMS

MEI, Haijuan, LUO, Quanshun <http://orcid.org/0000-0003-4102-2129>, HUANG, Xueli, DING, Ji Cheng, ZHANG, Teng Fei <http://orcid.org/0000-0003-3819-4042> and WANG, Qimin

Influence of lubricious oxides formation on the tribological behavior of Mo-V-Cu-N coatings deposited by HIPIMS

Haijuan Mei [a,b], Quanshun Luo [b], Xueli Huang [a], Ji Cheng Ding [c],

Teng Fei Zhang [a,*], Qimin Wang [a,*]

[a] *School of Electromechanical Engineering, Guangdong University of Technology, Guangzhou, China*

[b] *Materials and Engineering Research Institute, Sheffield Hallam University, Sheffield, S1 1WB, UK*

[c] *School of Convergence Science, Pusan National University, Busan 609-735, South Korea*

Abstract

The variations of microstructure, mechanical properties, and oxidation behavior of Mo-V-Cu-N coatings are directly correlated to the chemical compositions, which significantly affects their tribological behavior. The aim of this work was to characterize Mo-V-Cu-N coatings with different chemical compositions deposited by high power impulse magnetron sputtering (HIPIMS) using single Mo-V-Cu segmental target, and to investigate the correlations between the lubricative oxides formed on coating surfaces with the variation of tribological behavior at different temperatures. The oxidation of Mo-V-Cu-N coatings started at 400 °C with the lubrication oxides of Mo-O and Cu-Mo-O were formed, which led to the decrease in coefficients of friction and wear rates of the coatings. It was found that the rapid outward diffusion of Mo and Cu atoms took place preferentially at around the growth defects (e.g. microparticles and pores). The incorporation of V atoms into Mo-Cu-N coatings enhanced the oxidation resistance at temperatures below 400 °C. At 500 °C, all the fcc B1-MoN and VN phases disappeared due to the severe oxidation, and the V_2O_5 phase was first appeared. Even though a relatively low coefficient of friction was obtained at 500 °C, the wear resistance of Mo-V-Cu-N coatings was decreased due to the severe oxidation and loss of mechanical strength.

Keywords: Mo-V-Cu-N; Low friction; Lubricious oxides; Tribological behavior.

* Corresponding author: tfzhang@gdut.edu.cn (Teng Fei Zhang);

qmwang@gdut.edu.cn (Qimin Wang).

1 Introduction

With the increasing requirements of modern processing conditions, especially for the high-speed and dry machining, self-lubrication coatings have been put forward to reduce the friction and wear between the coated tools and the machining workpieces. Recently, binary molybdenum nitride (MoN) coatings have attracted much attentions, which exhibit excellent wear resistance due to the unique combination of mechanical properties of Mo-nitride and the lubricating effects of Mo-oxides [1–4]. The mechanical and tribological properties of Mo-N coatings can be improved by addition other elements [5–7]. For example, by incorporation of copper (Cu) atoms into Mo-N coatings, the average coefficient of friction (COF) could be further decreased from 0.4 to 0.2, which was attributed to the formation of lubricating $CuMoO_4$ oxide [7]. It was reported that the COF could be reduced by the double oxides from binary alloy system [8]. Due to the differences in ionic potential of MoO_3 and CuO [9], the ternary oxides (e.g. $CuMoO_4$) could exhibit a lower COF than their binary oxides. However, the high-temperature tribological behavior of Mo-Cu-N coating system has been rarely investigated. It has been reported that the tribological effectiveness of Mo-N coatings was restricted to a maximum temperature of 500 °C due to the formation of volatile oxides MoO_3 [10]. To enhance the tribological properties at elevated temperatures, vanadium (V) has been incorporated into hard coatings, which offers the lubricating effects due to vanadium oxides (also referred as Magnéli phases) formed at high temperatures above 500 °C [11–14]. In addition, due to the lubricious oxide V_2O_5 has a low melting point at around 680 °C, the COF can be further reduced at higher temperatures by the effect of liquid lubrication [15, 16]. It is well known that multicomponent alloying in coatings with different elements have combined the

advantage of each alloying element, which could significantly improve the comprehensive performance of the coatings.

Thus, it is inferred that the Mo-Cu-N coatings could be alloyed with V element to form quaternary Mo-Cu-V-N coatings. In our previous works [17, 18], Mo-Cu-V-N coatings with V content less than 2.5 at.% exhibited a low COF of 0.3 and excellent wear rate of 10^{-17} $m^3/N \cdot m$ at room-temperature tribological test due to the formation of mixed lubricious oxides of MoO_2, CuO and V_2O_5. As for the MoN [10] and VN coatings [15], the effect of formation and melting of Mo-O and V-O oxides on the high-temperature tribological behavior has been widely investigated. It was found that the initial decrease in COF of VN coatings occurred at 400 °C, and the lowest COF of 0.25 was achieved at 700 °C due to the formation and melting of V_2O_5 oxide, leading to liquid lubrication. However, the forming type of lubricious oxides and their influence on the high-temperature tribological performance of Mo-V-Cu-N coatings have not been sufficiently explored. Therefore, in this study, Mo-V-Cu-N coatings with different chemical compositions were synthesized and their microstructure, mechanical, oxidation and high-temperature tribological behavior were studied. The correlations between the lubricative oxides formed on coating surfaces with the variation of tribological behavior at different temperatures were also investigated.

2 Experimental

2.1 Coating deposition

Mo-V-Cu-N coatings were deposited on 316L stainless steel and cemented carbide substrates by HIPIMS using a rectangular Mo-V-Cu segmental target (99.9%

purity, 69 mm × 443 mm), which was consisted of three pure metal targets of Mo, V and Cu. A schematic diagram of the Mo-V-Cu segmental target and substrate locating position is shown in Fig. 1. Two different vertical substrate positions (sample 1 and sample 2) were used to deposit the Mo-V-Cu-N coatings with different chemical compositions. Stainless steel substrates were coated for residual stress tests, and cemented carbide substrates were coated mainly for the tests of mechanical and tribological properties. Prior to the deposition, all the substrates were ultrasonically cleaned with acetone and alcohol, then placed on the vertical substrate holder with a horizontal distance of 120 mm from the target. During deposition, the vacuum chamber was pumped down to a base pressure of 5.0×10^{-3} Pa, and the working temperature was set up to 200 °C. To remove surface contaminates, the substrates were first etched by Ar plasma with a DC bias of −1000 V for 20 min. To improve the adhesion between substrate and coating, a thin CrN adhesion layer with a thickness of ~300 nm was deposited by arc ion plating. Then the Mo-V-Cu-N coatings were deposited by HIPIMS with a target power of 1.0 kW and a duty cycle of 3%. The detail deposition parameters are listed in Table 1.

2.2 Coating characterization

The surface and cross-sectional morphology of the coatings were characterized using a scanning electron microscope (SEM, FEI Quanta650), and the chemical compositions were determined by the energy-dispersive X-ray spectroscopy (EDS) system. A grazing incidence X-ray diffraction (XRD, Empyrean) with Co K_{α} radiation was used to investigate the phase structure of as-deposited Mo-V-Cu-N coatings and to identify the oxide phases formed after high-temperature tribological tests. All the XRD measurements were carried out at 40 kV and 40 mA with a fixed incident angle

of 4°, and the scanning ranged from 20° to 85° with a step size of 0.02°. The residual stress of as-deposited coatings was measured by film stress tester (FST-1000, Supro Instruments) according to substrate curvature method based on Stoney's equation [19]. Hardness and elastic modulus of as-deposited coatings were carried out on cemented carbide substrates by nanoindentation tester (NHT^2, CSM). The effective indentation depth was kept less than 10% of the coating thickness to minimize the substrate effect. The adhesion strength of the coatings was measured by a scratch tester (RST, CSM) at a load linearly increasing to 80 N. The tribological properties of both coatings were investigated by using a ball-on-disc tribometer (THT, CSM) with Al_2O_3 ball (Ø 6 mm) at room temperature (RT), 300 °C, 400 °C and 500 °C, respectively. The tests were carried out under a load of 2 N and a rotational speed of 400 r/min. During high-temperature tribological tests, the temperatures of the coated samples were controlled by a heating module and an indirect water cooling system, which were measured through the way of contact conduction by thermocouple (fixed and contact at the center of substrate backfaces during rotating-sliding test). Two-dimensional (2D) cross-sectional profile of the wear tracks were examined by a laser scanning confocal microscope (OLS4100, Olympus), then the wear rates were calculated based on the worn volume.

3 Results and discussion

3.1 Microstructure and mechanical properties

To simplify the notations, both coatings were normalized to 50 at.% of nitrogen. The nominal concentrations of Mo-V-Cu-N coatings were assigned as

$Mo_{0.71}V_{0.24}Cu_{0.05}N$ and $Mo_{0.76}V_{0.08}Cu_{0.16}N$, corresponding to the sample 1 and sample 2 coatings (Fig. 1), respectively. As shown in Fig. 2, three diffraction peaks at 36.9°, 42.7° and 62.4° were observed, corresponding to the (111), (200) and (220) peaks of a face-centered-cubic (FCC) phase. Both coatings showed a high preferred orientation of the (200) texture, especially for the $Mo_{0.76}V_{0.08}Cu_{0.16}N$ coating. The diffraction peaks showed a clear asymmetric shape, and higher V content led to more obvious asymmetric trend. It indicated that the peaks were convolution peaks that composed of another NaCl-type phase in the coatings, which was identified to be the VN phase. It was considered that the V firstly formed a solid solution in MoN lattice, and the excess V segregated and formed an individual VN phase. To analyze the FCC Mo-N and VN phases, the diffraction peaks were fitted by Gaussian profiles. The lattice parameters of Mo-N and VN were then calculated by the fitted diffraction peaks, which were listed in Table 2. It was found that the lattice parameters of Mo-N phase ranged from 4.19 Å to 4.22 Å for both coatings. Thus, the FCC Mo-N phase should be assigned as B1-MoN phase with lattice parameters in the range of 4.19–4.27 Å [20]. In addition, the VN phase with low diffraction intensity also could be found, and the calculated lattice parameters were in the range from 4.12 to 4.13 Å. While no diffraction peaks of Cu phase were observed in both coatings, indicating that the Cu atoms distributed interstitially within the nanocrystalline Mo-N phases or in an amorphous state [7, 21]. When comparing these two coatings, it was found that the peaks shifted toward higher diffraction angles for $Mo_{0.76}V_{0.08}Cu_{0.16}N$ coating with higher Cu content, indicating a relaxation of compressive residual stress [6]. In addition, peak broadening was also observed in the $Mo_{0.76}V_{0.08}Cu_{0.16}N$ coating, implying that lattice distortion or grain refining.

Fig. 3 compares the surface and cross-sectional morphologies of both coatings. As shown in Fig. 3(a), many microparticles could be observed on $Mo_{0.71}V_{0.24}Cu_{0.05}N$ coating surface, which was typical growth defects formed during deposition. However, Mo-Cu-V-N composite coatings deposited by similar HIPIMS technique exhibited a smooth surface without any microparticles in our previous study [17]. It indicated that these microparticles were mainly produced during the deposition of CrN adhesion layer by arc ion plating. As for $Mo_{0.76}V_{0.08}Cu_{0.16}N$ coating surface (see Fig. 3(b)), the density of microparticles significantly decreased, which was considered to be attributed to the increase of Cu content in the coating. Due to Cu atoms has much higher sputtering yield than that of Mo and V atoms during coating deposition [22], the deposition rate and atomic mobility could be increased on the growing surface at higher Cu contents, which would lead to many underlayer microparticles were gradually covered by the upper surface coatings. However, the $Mo_{0.76}V_{0.08}Cu_{0.16}N$ coating with higher Cu contents exhibited a (Fig. 3(d)) coarser column structure (Fig. 3(f)). Based on the coating thickness measured from the cross-sectional images, it was found that a higher deposition rate of 10.8 nm/min was achieved for the $Mo_{0.76}V_{0.08}Cu_{0.16}N$ coating, compared to that of the $Mo_{0.71}V_{0.24}Cu_{0.05}N$ coating (5.6 nm/min).

The mechanical properties of Mo-V-Cu-N coatings were listed in Table 3. It could be found that both coatings presented a high compressive residual stress, especially for the $Mo_{0.71}V_{0.24}Cu_{0.05}N$ coating. While the residual stress could be released by the presence of a ductile copper phase in the coatings [6]. The coating hardness of $Mo_{0.71}V_{0.24}Cu_{0.05}N$ coating and $Mo_{0.76}V_{0.08}Cu_{0.16}N$ coating were in the range of 30.6 ± 0.8 GPa and 23.4 ± 0.9 GPa, respectively. It is well known that the

hardness and elastic modulus are related to the chemical compositions, microstructure, and residual stress of the coatings [23–25]. Thus, the decrease in hardness for $Mo_{0.76}V_{0.08}Cu_{0.16}N$ coating could be mainly due to the combined effects of coarse microstructure, relaxation of compressive residual stress, and higher Cu contents in the coating. In addition, it was reported that the H^3/E^{*2} ratios could be used to predict the resistance against plastic deformation [26]. It was shown that a higher H^3/E^{*2} ratio of 0.13 was achieved for the $Mo_{0.71}V_{0.24}Cu_{0.05}N$ coating, indicating that a better wear resistance as compared to the $Mo_{0.76}V_{0.08}Cu_{0.16}N$ coating. While the $Mo_{0.76}V_{0.08}Cu_{0.16}N$ coating exhibited a higher adhesion strength of 35.4 N than that of the $Mo_{0.71}V_{0.24}Cu_{0.05}N$ coating, which was attributed to the decrease of compressive residual stress from 5.2 to 2.9 GPa. It was reported that a high compressive residual stress resulted in the reduction of adhesion strength [27].

3.2 Oxidation behavior

Fig. 4 compares the sample temperatures and oven temperatures during sliding tested at room temperature (RT), 300 °C, 400 °C and 500 °C, respectively. At RT, the sample temperature was controlled in a small range of 25–26 °C, whereas the oven temperature was kept at a constant temperature of 29 °C. When the temperature increased above 300 °C, it was found that all the sample temperatures were controlled well within a control error less than 5 °C. However, all the oven temperatures were about 70 °C higher than that of the sample temperatures, which would affect the oxidation on the coating surfaces.

To fully understand the types of formed lubricious oxides of $Mo_{0.71}V_{0.24}Cu_{0.05}N$ and $Mo_{0.76}V_{0.08}Cu_{0.16}N$ coatings, the XRD patterns of coating surfaces were carried

out outside the wear track after tribological tests at different temperatures, as shown in Fig. 5. The patterns of both coatings showed no significant changes in structure with increasing the temperature up to 300 °C. After tribological test at 400 °C, the $Mo_{0.71}V_{0.24}Cu_{0.05}N$ coating (see Fig. 5(a)) was slightly oxidized to form dominate oxide phase of Mo_4O_{11} and a minor phase of Mo_8O_{23}, which were corresponded to the lubricious Magnéli phases series Mo_nO_{3n-1} [28]. In addition, a minor oxide phase of $Cu_3Mo_2O_9$ (JCPDS 24-0055) could also be identified, indicating the onset of oxidation at this temperature. As for the $Mo_{0.76}V_{0.08}Cu_{0.16}N$ coating (see Fig. 5(b)), it was found that more oxide phases formed including a few new peaks of MoO_3, Mo_9O_{26}, $CuMoO_4$ and $Cu_6Mo_5O_{18}$ being identified, which was caused by a severe oxidation of the coating surface. It should be noted that the copper molybdate phases identified here might be one of the nonstoichiometric copper molybdates ($Cu_xMo_yO_{4-z}$) [29–32]. As the temperature increased up to 500 °C, all the B1-MoN and VN phases disappeared, replaced by various oxides of Mo-O, Cu-Mo-O, Cu-O and V-O on the coating surfaces, indicating that both coatings were completely oxidized, which was consistent with the EDS results of the coating surfaces in Table 4. As for the $Mo_{0.71}V_{0.24}Cu_{0.05}N$ coating, dominant oxide phases of Mo_4O_{11}, MoO_3 and V_2O_5 and minor Cu-Mo-O oxides were identified. It was reported that since there was an excess Mo in the Cu-Mo coatings by Ion-beam deposition (IBD), all the Cu would eventually transform to $CuMoO_4$ phase, with excess Mo oxidized to MoO_3 [33]. For the $Mo_{0.76}V_{0.08}Cu_{0.16}N$ coating with higher Cu contents, it was observed that mainly phases of Mo_4O_{11}, Mo_9O_{26} and Cu-Mo-O oxides were formed on the coating surface.

To further investigation of the high-temperature oxidation behavior, the coating surfaces outside wear tracks were analyzed by SEM after tribological tests at 300 °C,

400 °C and 500 °C, respectively. Fig. 6 shows the surface morphologies and EDS linescan profiles of $Mo_{0.71}V_{0.24}Cu_{0.05}N$ coating, it could be seen that some slightly oxidized microparticles appeared on the coating surface at 300 °C (see Fig. 6(a)), which was considered to be affected by the higher oven temperature of ~370 °C. The magnified image of oxidized particle was presented in Fig. 6(b), it was found that the oxidized particle with a diameter of ~4.1 μm was covered with a thin oxide layer, which was composed of Cu-Mo-O oxides detected by the EDS linescan in Fig. 6(c). At 400 °C, the coating surface suffered heavier oxidation, as shown in Fig. 6(d). It could be seen that the oxidized particle was uniformly covered with a thick honeycomb-like structure (see Fig. 6(e)), corresponding to the oxide phase of $Cu_3Mo_2O_9$ based on the EDS linescan and above XRD results. Moreover, it is interesting to find that various Mo-O oxides mainly composed of Mo_4O_{11} and Mo_8O_{23} phases distributed at around the oxidized particle and formed a circular-like structure. Such oxidation behavior indicated that the rapid outward diffusion of Mo and Cu elements, which preferentially spread outward at around growth defects (e.g. microparticles and pores). Similar results were also reported by Panjan et al. [14] that the outward diffusion of V took place through voids presented at the growth defects. When the temperature increased up to 500 °C, the coating surface was almost completely oxidized and covered with circular-like oxides in a large diameter of ~40 μm (see Fig. 6(g)–(h)). The particles in the center were mainly oxidized to form Cu-Mo-O oxides, which was identified by the EDS linescan in Fig. 6(i). Moreover, some oxides with large crystal grains formed in the pore defects, as shown in Fig. 6(j). This phenomenon strongly indicated that the rapid outward diffusion of Mo and Cu elements occurred at high temperatures, which were preferential spread at around the

growth defects.

Fig. 7 presents the surface morphologies and EDS linescan of the $Mo_{0.76}V_{0.08}Cu_{0.16}N$ coating after tribological tests at 300 °C, 400 °C and 500 °C. At 300 °C, similar oxidized particles with a diameter of ~4.0 μm could be observed on $Mo_{0.76}V_{0.08}Cu_{0.16}N$ coating surface in Fig. 7(a)–(c). As the temperature increased up to 400 °C, the coating surface was uniformly covered with many cluster oxides in Fig. 7(d)–(e)). The EDS linescan profile in Fig. 7(f) revealed that the cluster oxides were mostly composed of Cu-Mo-O oxides. Based on the EDS analysis and XRD results, oxides formed inside the circular-like structure were mainly composed of Mo-O oxides. As the temperature further increased to 500 °C, the coating surface had been completely oxidized to form the oxides with larger crystal grains in Fig. 7(g)–(h). To further identify the types of oxides, the oxides were peeled off from the coating surface by conductive adhesive. As shown in Fig. 8, the EDS analysis revealed that these oxides were mainly corresponded to Cu-Mo-O phase, which was consistent with the EDS linescan results in Fig. 7(i). As compared to $Mo_{0.71}V_{0.24}Cu_{0.05}N$ coating, the EDS analysis of coating surface (see Table 4) revealed that the $Mo_{0.76}V_{0.08}Cu_{0.16}N$ coating suffered harsher oxidation, which could be due to the coarse column microstructure and the increase of Mo and Cu contents in the coatings. It was inferred that the incorporation of V element into Mo-Cu-N coating system could improve the oxidation resistant at certain temperature ranges.

3.3 Tribological behavior

The effect of test temperature on the COF of the coatings was showed in Fig. 9. Both coatings exhibited a similar tribological behavior. It was found that the lowest

COF of 0.36 and 0.32 were achieved at room temperature (RT) for the $Mo_{0.71}V_{0.24}Cu_{0.05}N$ and $Mo_{0.76}V_{0.08}Cu_{0.16}N$ coatings, respectively. However, obvious fluctuations were observed in the friction curves at 300 °C for both coatings, which could be due to the initial generation of wear particles, and the subsequent formation of a tribofilm in the wear track [34]. As the temperature further increased to above 400 °C, the COF decreased to 0.50 and 0.38 for $Mo_{0.71}V_{0.24}Cu_{0.05}N$ and $Mo_{0.76}V_{0.08}Cu_{0.16}N$ coatings, respectively. The decrease in COF could be attributed to the lubricious oxides formed on wear track surfaces. As shown in Fig. 9(c), the $Mo_{0.76}V_{0.08}Cu_{0.16}N$ coating generally exhibited a lower COF than that of the $Mo_{0.71}V_{0.24}Cu_{0.05}N$ coating except for 300 °C, which was attributed to the severe oxidation and larger fraction of Cu-Mo-O lubricious oxides. Similar results were reported that the larger fraction of $CuMoO_4$ lubricious oxides formed on the worn surface resulted in a lower COF [7].

To investigate the wear mechanism of Mo-V-Cu-N coatings, the worn surfaces were analyzed in details after tribological tests at RT, 300 °C, 400 °C and 500 °C. As shown in Fig. 10(a), it can be clearly seen that the wear track was relatively narrow with wear debris accumulated at both sides of the wear track on the $Mo_{0.71}V_{0.24}Cu_{0.05}N$ coating after tribological test at RT. Moreover, some furrows and scratches formed along the sliding direction inside the wear track in Fig. 10(e), which indicated that mild abrasive wear occurred at RT. In addition, the EDS analysis of the worn surfaces (see Table 5) revealed that the worn surface was slightly oxidized, indicating that mild oxidation wear also occurred at RT, resulting in a low COF of ~0.3. Similar results have been identified by XPS analysis in our previous work [17]. While for the $Mo_{0.76}V_{0.08}Cu_{0.16}N$ coating, it was observed that the worn surface was

much smoother without obvious wear debris observed on either side of the wear track (see Fig. 10(i)). The magnified image of wear track exhibited a shallow worn surface with slight scratches (Fig. 10(m)), indicating a better tribological performance as compared to the $Mo_{0.71}V_{0.24}Cu_{0.05}N$ coating. In addition, some compacted particles were presented on worn surfaces, which were compacted by the counterpart during sliding process.

As the temperature increased to 300 °C, the worn surface of $Mo_{0.71}V_{0.24}Cu_{0.05}N$ coating became much rougher with many adhesion debris formed on wear track, as shown in Fig. 10(b, f), which indicated that adhesion wear occurred at 300 °C. Similar tribological behavior was also observed for $Mo_{0.76}V_{0.08}Cu_{0.16}N$ coating in Fig. 10(j), and obvious cracks could be found in the magnified image (see Fig. 10(n)). Such cracks were typically observed in the sliding contact conditions of hard materials that experienced large surface tractions, which resulted in a high COF [35]. The sharp increase in friction curves observed at the beginning sliding periods of ~500 cycles for both coatings at 300 °C (Fig. 9) could be due to the rough coating surfaces formed with some oxidized microparticles. However, after further sliding process, the microparticles were compacted or worn off, and the worn surfaces were gradually oxidized due to friction heating on the contact area. It was identified by the high O contents of ~44.7 at.% detected on worn surfaces for both coatings, which was almost twice higher than those of the coating surfaces outside the wear tracks, as listed in Table 4 and Table 5. Thus, the formed oxidized debris were compacted and scratched by the counterpart (Al_2O_3 ball) during cycle sliding process, leading to some cracks and adhesion debris formed on the worn surfaces (see Fig. 10(f, n)). It was reported that the production of wear debris with large diameters interacted with both surfaces

by scratching or getting crushed in the contact area [36]. Such tribological behavior was typical for abrasive and adhesion wear, which led to a high COF and wear rate at 300 °C.

After tribological tests at 400 °C, smooth compacted debris formed on the wear track of $Mo_{0.71}V_{0.24}Cu_{0.05}N$ coating in Fig. 10(c, g). While for $Mo_{0.76}V_{0.08}Cu_{0.16}N$ coating, ball-like particles appeared inside the wear debris in Fig. 10(k, o), which could be due to the oxidized particles were compacted under cycle sliding load. In addition, the EDS analysis revealed that the worn surfaces of both coatings were almost completely oxidized, indicating that mainly oxidation wear occurred at 400 °C. As compared to 300 °C, the COF decreased at 400 °C, which was attribute to the formed lubricious oxides of Mo-O and Cu-Mo-O, as discussed above. It was reported that the oxides of $CuMoO_4$ and MoO_3 were expected to soften between 200 °C and 550 °C, which led to the COF dropped in this temperature range [33].

When the temperature further increased up to 500 °C, the worn surface of $Mo_{0.71}V_{0.24}Cu_{0.05}N$ coating was completely oxidized to form a porous tribofilm (see Fig. 10(d, h)), which could be related to the severe oxidation of worn surface, especially for the pore defects, as observed in Fig. 6(j). In addition, a small amount of Cr content on worn surface was detected by the EDS analysis (see Table 5), implying that the coating surface was almost been worn out and the damage reached to the CrN adhesion layer during sliding process. While for the $Mo_{0.76}V_{0.08}Cu_{0.16}N$ coating in Fig. 10(l), the wear track was relatively smooth and wider as compared to the $Mo_{0.71}V_{0.24}Cu_{0.05}N$ coating at 500 °C. The magnified image exhibited a compacted worn surface with thick oxide scales in Fig. 10(p), which could be demonstrated as severe oxidation wear at 500 °C. As shown in Fig. 11, the debris outside the wear

track of $Mo_{0.76}V_{0.08}Cu_{0.16}N$ coating was further investigated. It was found that the wear debris were mainly composed of Cu-Mo-O oxides, which was consistent with the oxidation behavior shown in Fig. 8. Moreover, the chemical compositions of spectrum 1 in Fig. 11(b) revealed that the block debris mainly peeled off from the coatings during wear test. Due to the severe oxidation wear occurred at 500 °C, the loss of mechanical strength and stability, leading to the soft oxides being easily worn out from the wear tracks.

After tribological tests at different temperatures, the wear rates of both coatings were compared in Fig. 12. It was found that $Mo_{0.71}V_{0.24}Cu_{0.05}N$ and $Mo_{0.76}V_{0.08}Cu_{0.16}N$ coatings exhibited a relatively low wear rate of 6.5×10^{-17} and 4.7×10^{-17} $m^3/N \cdot m$ at RT, respectively. A better wear resistant was achieved for the $Mo_{0.76}V_{0.08}Cu_{0.16}N$ coating, which could be attributed to the increase of Cu content and the relaxation of residual stress. It was reported that the wear rate was correlated to the adhesion energy, which was directly related to the residual stress and ultimately, the initial copper content [6]. A relatively high wear rate of 10^{-15} $m^3/N \cdot m$ was achieved at 300 °C for both coatings, which would be due to the wear mechanism dominated by adhesion and abrasive wear. Due to the lubricious oxides of Mo-O and Cu-Mo-O were formed at 400 °C, the wear rates of both coatings decreased slightly. As the temperature further increased to 500 °C, the highest wear rate of 10^{-14} $m^3/N \cdot m$ was achieved for both coatings, the rapid decrease in wear resistant was mainly due to the severe oxidation and the loss of mechanical strength of both coatings. Similar results were reported by Luo et al. that the accelerated oxidation of TiAlN/VN coatings at first led to the massive generation of oxide debris at 500 °C, and then to a fast deterioration of the coatings despite the lowest COF was achieved at 700 °C [12].

4 Conclusions

In this work, microstructure, mechanical, oxidation and high-temperature tribological behavior of $Mo_{0.71}V_{0.24}Cu_{0.05}N$ and $Mo_{0.76}V_{0.08}Cu_{0.16}N$ coatings were studied. The correlations between the lubricative oxides formed on coating surfaces with the variation of tribological behavior at different temperatures were also investigated. Both coatings exhibited FCC B1-MoN and VN phases with (200) preferred orientation, and showed similar oxidation and tribological behavior. It was found that the lowest COF of ~0.3 and wear rate of 10^{-17} $m^3/N{\cdot}m$ were achieved at RT for both coatings, which could be attribute to the mild abrasive and oxidation wear. The highest COF of ~0.68 was achieved at 300 °C, resulting in a high wear rate of 10^{-15} $m^3/N{\cdot}m$ due to the adhesion and abrasive wear. At 400 °C, the lubrication oxides of Mo-O and Cu-Mo-O first appeared on both coating surfaces, which led to the decrease in COF and wear rate. Due to severe oxidation wear and the loss of mechanical strength of both coatings at 500 °C, the highest wear rate of 10^{-14} $m^3/N{\cdot}m$ was obtained despite of a lower COF of ~0.38.

Comparing two coatings, despite of a lower COF achieved for $Mo_{0.76}V_{0.08}Cu_{0.16}N$ coating, the wear resistant was compromised by the formation of lubricious oxides at high temperatures, which could be due to the loss of mechanical strength of the coatings. Thus, it could be inferred that an excellent wear resistant coatings should combine both low COF and low wear rate, which were determined by lubricious oxides and mechanical strength.

Acknowledgements

The work was supported by the projects of National Natural Science Foundation of China (51522502, 51875109), China Postdoctoral Science Foundation funded project (2016M600641) and Guangdong Natural Science Funds (2016A050502056).

References

[1] M.K. Kazmanli, M. Ürgen, A.F. Cakir, Effect of nitrogen pressure, bias voltage and substrate temperature on the phase structure of Mo-N coatings produced by cathodic arc PVD, Surf. Coat. Technol. 167 (2003) 77–82.

[2] I. Jauberteau, A. Bessaudou, R. Mayet, J. Cornette, J.L. Jauberteau, P. Carles, T. Méjean, Molybdenum nitride films: crystal structures, synthesis, mechanical, electrical and some other properties, Coatings 5 (2015) 656–687.

[3] T. Wang, G. Zhang, S. Ren, B. Jiang, Effect of nitrogen flow rate on structure and properties of MoNx coatings deposited by facing target sputtering, J. Alloy. Compd. 701 (2017) 1–8.

[4] B. Bouaouina, A. Besnard, S.E. Abaidia, A. Airoudj, F. Bensouici, Correlation between mechanical and microstructural properties of molybdenum nitride thin films deposited on silicon by reactive R.F. magnetron discharge, Surf. Coat. Technol. 333 (2018) 32–38.

[5] J.N. Kim, S. Park, T. Kim, J.J. Lee, Structure and mechanical properties of Mo-N/Cu films produced by inductively coupled plasma reactive sputtering, Thin Solid Films 519 (2011) 6876–6880.

[6] K.E. Pappacena, D. Singh, O.O. Ajayi, J.L. Routbort, O.L. Erilymaz, N.G. Demas, G. Chen, Residual stresses, interfacial adhesion and tribological properties of MoN/Cu composite coatings, Wear 278–279 (2012) 62–70.

[7] J.H. Shin, Q.M. Wang, K.H. Kim, Microstructural evolution and tribological behavior of Mo-Cu-N coatings as a function of Cu content, Mater. Chem. Phys.

130 (2011) 870–879.

[8] W. Gulbiński, T. Suszko, W. Sienicki, B. Warcholiński, Tribological properties of silver- and copper-doped transition metal oxide coatings, Wear 254 (2003) 129–135.

[9] A. Öztürk, K.V. Ezirmik, K. Kazmanlı, M. Ürgen, O.L. Eryılmaz, A. Erdemir, Comparative tribological behaviors of TiN, CrN and MoNCu nanocomposite coatings, Tribol. Int. 41 (2008) 49–59.

[10] G. Gassner, P.H. Mayrhofer, K. Kutschej, C. Mitterer, M. Kathrein, Magnéli phase formation of PVD Mo-N and W-N coatings, Surf. Coat. Technol. 201 (2006) 3335–3341.

[11] K. Kutschej, P.H. Mayrhofer, M. Kathrein, P. Polcik, C. Mitterer, Influence of oxide phase formation on the tribological behaviour of Ti-Al-V-N coatings, Surf. Coat. Technol. 200 (2005) 1731–1737.

[12] Q. Luo, Temperature dependent friction and wear of magnetron sputtered coating TiAlN/VN, Wear 271 (2011) 2058–2066.

[13] R. Franz, C. Mitterer, Vanadium containing self-adaptive low-friction hard coatings for high-temperature applications: A review, Surf. Coat. Technol. 228 (2013) 1–13.

[14] P. Panjan, A. Drnovšek, J. Kovač, M. Čekada, M. Panjan, Oxidation processes in vanadium-based single-layer and nanolayer hard coatings, Vacuum 138 (2017) 230–237.

[15] N. Fateh, G.A. Fontalvo, G. Gassner, C. Mitterer, Influence of high-temperature oxide formation on the tribological behaviour of TiN and VN coatings, Wear 262 (2007) 1152–1158.

[16] P.H. Mayrhofer, P.E. Hovsepian, C. Mitterer, W.D. Münz, Calorimetric evidence for frictional self-adaptation of TiAlN/VN superlattice coatings, Surf. Coat. Technol. 177–178 (2004) 341–347.

[17] H.J. Mei, S.S. Zhao, Z.T. Wu, W. Dai, Q.M. Wang, Effect of nitrogen partial pressure on microstructure and mechanical properties of Mo-Cu-V-N composite coatings deposited by HIPIMS, Surf. Coat. Technol. 329 (2017) 68–76.

[18] H.J. Mei, R. Wang, X. Zhong, W. Dai, Q.M. Wang, Influence of nitrogen partial pressure on microstructure and tribological properties of Mo-Cu-V-N composite coatings with high Cu content, Coatings 8 (2018) 24.

[19] G.G. Stoney, The tension of metallic films deposited by electrolysis, Proc. R. Soc. Lond. Ser. A 82 (1909) 172–175.

[20] H. Ihara, Y. Kimura, K. Senzaki, H. Kezuka, M. Hirabayashi, Electronic structures of B1MoN, fcc Mo_2N, and hexagonal MoN, Phys. Rev. B 31 (1985) 3177–3178.

[21] A. Erdemir, A crystal chemical approach to the formulation of self-lubricating nanocomposite coatings, Surf. Coat. Technol. 200 (2005) 1792–1796.

[22] N. Laegreid, G.K. Wehner, Sputtering Yields of Metals for Ar+ and Ne+ Ions with Energies from 50 to 600 ev, J. Appl. Phys. 32 (1961) 365–369.

[23] N. Bagcivan, K. Bobzin, G. Grundmeier, M. Wiesing, O. Ozcan, C. Kunze, R.H. Brugnara, Influence of HPPMS pulse length and inert gas mixture on the properties of (Cr,Al)N coatings, Thin Solid Films 549 (2013) 192–198.

[24] X.S. Wan, S.S. Zhao, Y. Yang, J. Gong, C. Sun, Effects of nitrogen pressure and pulse bias voltage on the properties of Cr–N coatings deposited by arc ion plating, Surf. Coat. Technol. 204 (2010) 1800–1810.

[25] P. Zeman, R. Cerstvý, P.H. Mayrhofer, C. Mitterter, Structure and properties of hard and superhard Zr-Cu-N nanocomposite coatings, J. Musil, Mater. Sci. Eng. A 289 (2000) 189–197.

[26] D.C. Tsai, Z.C. Chang, B.H. Kuo, C.T. Tsao, E.C. Chen, F.S. Shieu, Influence of discharge power on the structural, electro-optical, and mechanical properties of (TiZrHf)N coatings, J. Alloys Comp. 622 (2015) 446–457.

[27] H.J. Mei, S.S. Zhao, Q.M. Wang, Residual stress of TiN multilayer coatings alternately deposited by arc ion plating and magnetron sputtering, Nanosci. Nanotech. Let. 9 (2017) 885–891.

[28] A. Magnéli, Structures of the ReO_3-type with recurrent dislocations of atoms: 'homologous series' of molybdenum and tungsten oxides, Acta Cryst 6 (1953) 495–500.

[29] K. Nassau, S.C. Abrahams, The growth and properties of single crystal cupric molybdate, J. Cryst. Growth, 2 (1968) 136–140.

[30] K. Nassau, J.W. Shiever, Cupric oxide-molybdenum oxide phase diagram in air and in oxygen, J. Am. Ceram. Soc. 52 (1969) 36–40.

[31] I.D. Thomas, A. Herzog, D. Mclachlan, The crystallography of two compounds containing the oxides of copper and molybdenum, Acta Cryst 9 (1956) 316–317.

[32] L. Kihlborg, R. Norrestam, B. Olivecrona, The crystal structure of $Cu_3Mo_2O_9$, Acta Cryst B27 (1971) 2066–2070.

[33] K.J. Wahl, L.E. Seitzman, R.N. Bolster, I.L. Singer, M.B. Peterson, Ion-beam deposited Cu-Mo coatings as high temperature solid lubricants, Surf. Coat. Technol. 89 (1997) 245–251.

[34] Q. Luo, Origin of friction in running-in sliding wear of nitride coatings, Tribo. Lett. 37 (2010) 529–539.

[35] T.E. Fischer, Z. Zhu, H. Kim, D.S. Shin, Genesis and role of wear debris in sliding wear of ceramics, Wear 245 (2000) 53–60.

[36] K. Holmberg, A. Matthews, Coatings tribology: a concept, critical aspects and future directions, Thin Solid Films 253 (1994) 173–178.

Table 1 Deposition parameters of Mo-V-Cu-N coatings by HIPIMS.

Parameters	Values
Base pressure (Pa)	5.0×10^{-3}
Working pressure (Pa)	0.7
N_2 /Ar flow rate (sccm)	10 / 35
Working temperature (°C)	200
Bias voltage (V)	–100
Target power (kW)	1.0
Pulse length (μs)	150
Frequency (Hz)	200
Duty cycle	3%
Deposition time (min)	180

Table 2 Lattice parameters of Mo-V-Cu-N coatings.

Lattice parameter (Å)	$Mo_{0.71}V_{0.24}Cu_{0.05}N$	$Mo_{0.76}V_{0.08}Cu_{0.16}N$
B1-MoN	4.22 ± 0.01	4.19 ± 0.03
VN	4.13 ± 0.01	4.12 ± 0.01

Table 3 Characterizations of Mo-V-Cu-N coatings.

	$Mo_{0.71}V_{0.24}Cu_{0.05}N$	$Mo_{0.76}V_{0.08}Cu_{0.16}N$
Average coating thickness (μm)	1.3	2.3
Deposition rate (nm/min)	5.6 ± 0.2	10.8 ± 0.3
Residual stress (GPa)	–5.17 ± 0.09	–2.95 ± 0.03
Adhesion strength (N)	26.7 ± 1.3	35.4 ± 1.4
Hardness (GPa)	30.6 ± 0.8	23.4 ± 0.9
Elastic modulus (GPa)	443.4 ± 16.1	372.8 ± 22.8
H^3/E^{*2} ratio	0.13 ± 0.01	0.08 ± 0.02

Table 4 Chemical compositions of the coating surfaces outside the wear tracks after tribological tests at different temperatures.

Temperatures	Coatings	Chemical composition (at.%)				
		Mo	V	Cu	N	O
RT	$Mo_{0.71}V_{0.24}Cu_{0.05}N$	43.8	14.7	2.9	38.6	—
	$Mo_{0.76}V_{0.08}Cu_{0.16}N$	52.3	5.6	10.8	31.3	—
300 °C	$Mo_{0.71}V_{0.24}Cu_{0.05}N$	40.1	13.1	2.5	26.4	18.0
	$Mo_{0.76}V_{0.08}Cu_{0.16}N$	40.1	4.2	9.2	21.3	25.2
400 °C	$Mo_{0.71}V_{0.24}Cu_{0.05}N$	28.6	9.6	2.0	9.6	50.2
	$Mo_{0.76}V_{0.08}Cu_{0.16}N$	25.7	2.5	4.3	5.8	61.7
500 °C	$Mo_{0.71}V_{0.24}Cu_{0.05}N$	23.0	9.2	1.6	4.6	61.6
	$Mo_{0.76}V_{0.08}Cu_{0.16}N$	18.3	2.1	14.2	—	65.4

Table 5 Chemical compositions of the worn surfaces after tribological tests at different temperatures.

Temperatures	Wear tracks	Chemical composition (at.%)					
		Mo	V	Cu	N	O	Cr
RT	$Mo_{0.71}V_{0.24}Cu_{0.05}N$	42.5	14.3	2.8	30.7	9.7	—
	$Mo_{0.76}V_{0.08}Cu_{0.16}N$	47.3	5.4	9.8	25.1	12.4	—
300 °C	$Mo_{0.71}V_{0.24}Cu_{0.05}N$	31.2	10.3	1.9	11.9	44.7	—
	$Mo_{0.76}V_{0.08}Cu_{0.16}N$	30.2	3.1	6.2	5.7	54.8	—
400 °C	$Mo_{0.71}V_{0.24}Cu_{0.05}N$	27.7	9.5	1.4	4.7	56.7	—
	$Mo_{0.76}V_{0.08}Cu_{0.16}N$	27.3	2.9	4.2	—	65.6	—
500 °C	$Mo_{0.71}V_{0.24}Cu_{0.05}N$	24.3	8.3	1.5	—	64.4	1.5
	$Mo_{0.76}V_{0.08}Cu_{0.16}N$	25.4	3.1	4.6	—	66.9	—

List of figure captions

Fig. 1 Schematic diagram of Mo-V-Cu segmental target and the substrate locating position.

Fig. 2 XRD patterns and Gaussian fitting results of the as-deposited coatings.

Fig. 3 Surface and cross-sectional morphology of as-deposited Mo-V-Cu-N coatings: (a and e) $Mo_{0.71}V_{0.24}Cu_{0.05}N$, and (b and f) $Mo_{0.76}V_{0.08}Cu_{0.16}N$.

Fig. 4 Temperature curves as a function of sliding cycles at different temperatures: (a) RT, (b) 300 °C, (c) 400 °C, (d) 500 °C.

Fig. 5 XRD patterns of the Mo-V-Cu-N coatings after tribological tests at different temperatures: (a) $Mo_{0.71}V_{0.24}Cu_{0.05}N$, (b) $Mo_{0.76}V_{0.08}Cu_{0.16}N$.

Fig. 6 Surface morphologies and EDS linescan profiles of $Mo_{0.71}V_{0.24}Cu_{0.05}N$ coatings after tribological tests: (a)–(c) 300 °C, (d)–(f) 400 °C, and (g)–(i) 500 °C.

Fig. 7. Surface morphologies and EDS linescan profiles of $Mo_{0.76}V_{0.08}Cu_{0.16}N$ coatings after tribological tests: (a)–(c) 300 °C, (d)–(f) 400 °C, and (g)–(i) 500 °C.

Fig. 8 Surface oxides on $Mo_{0.76}V_{0.08}Cu_{0.16}N$ coating after tribological test at 500 °C: (a) oxides on conductive adhesive, (b) magnified image, (c) EDS plane-scan, and (d) chemical compositions.

Fig. 9 COF of Mo-V-Cu-N coatings at different temperatures: (a) $Mo_{0.71}V_{0.24}Cu_{0.05}N$, (b) $Mo_{0.76}V_{0.08}Cu_{0.16}N$, and (c) average COF.

Fig. 10 SEM micrographs of the worn surfaces of $Mo_{0.71}V_{0.24}Cu_{0.05}N$ (a–h) and $Mo_{0.76}V_{0.08}Cu_{0.16}N$ (i–p) coatings after tribological tests at different temperatures: (a, e,

i, m) RT, (b, f, j, n) 300 °C, (c, g, k, o) 400 °C, and (d, h, l, p) 500 °C.

Fig. 11 Debris outside the wear track of $Mo_{0.76}V_{0.08}Cu_{0.16}N$ coating after tribological test at 500 °C: (a) debris on conductive adhesive, (b) magnified image, (c) EDS plane-scan, and (d) chemical compositions.

Fig. 12 Wear rates of Mo-V-Cu-N coatings at different temperatures.

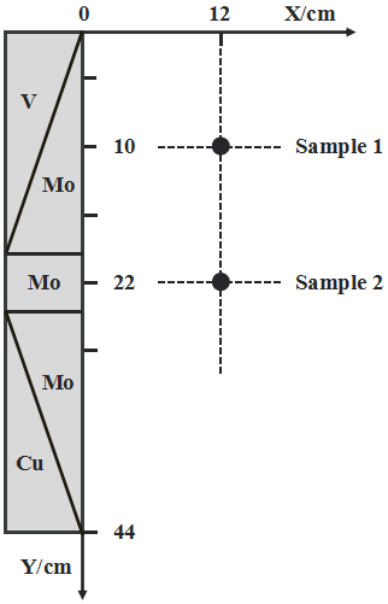

Fig. 1

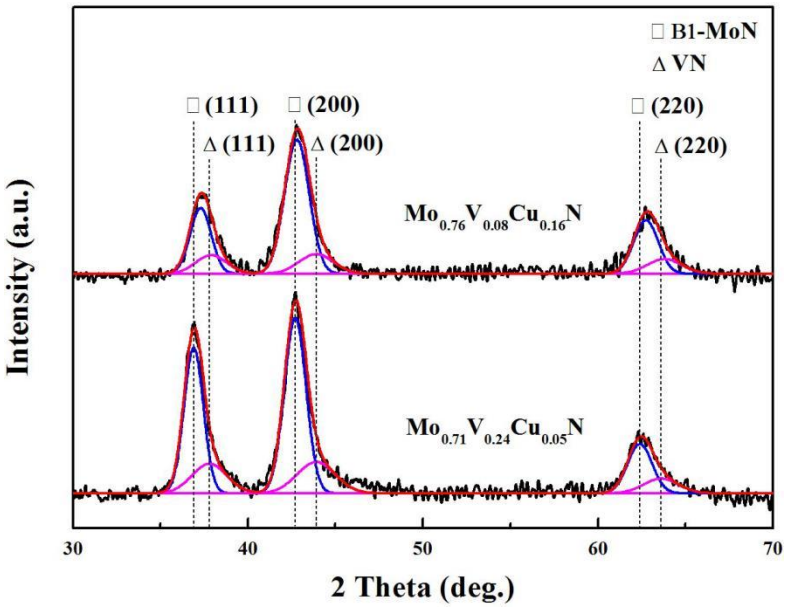
□ B1-MoN
Δ VN
□ (111)
□ (200)
□ (220)
Δ (111)
Δ (200)
Δ (220)
Mo0.76V0.08Cu0.16N
Mo0.71V0.24Cu0.05N
Intensity (a.u.)
30
40
50
60
70
2 Theta (deg.)

Fig. 2

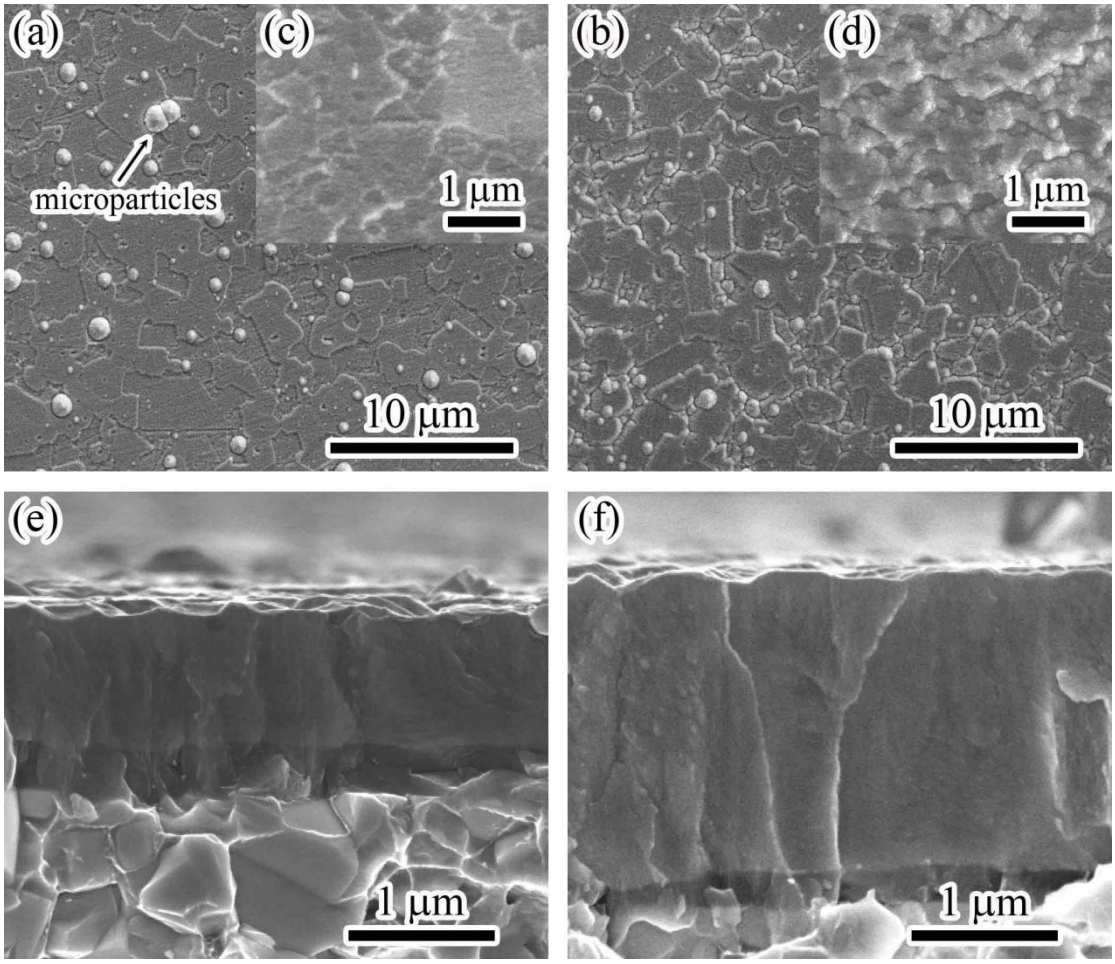

Fig. 3

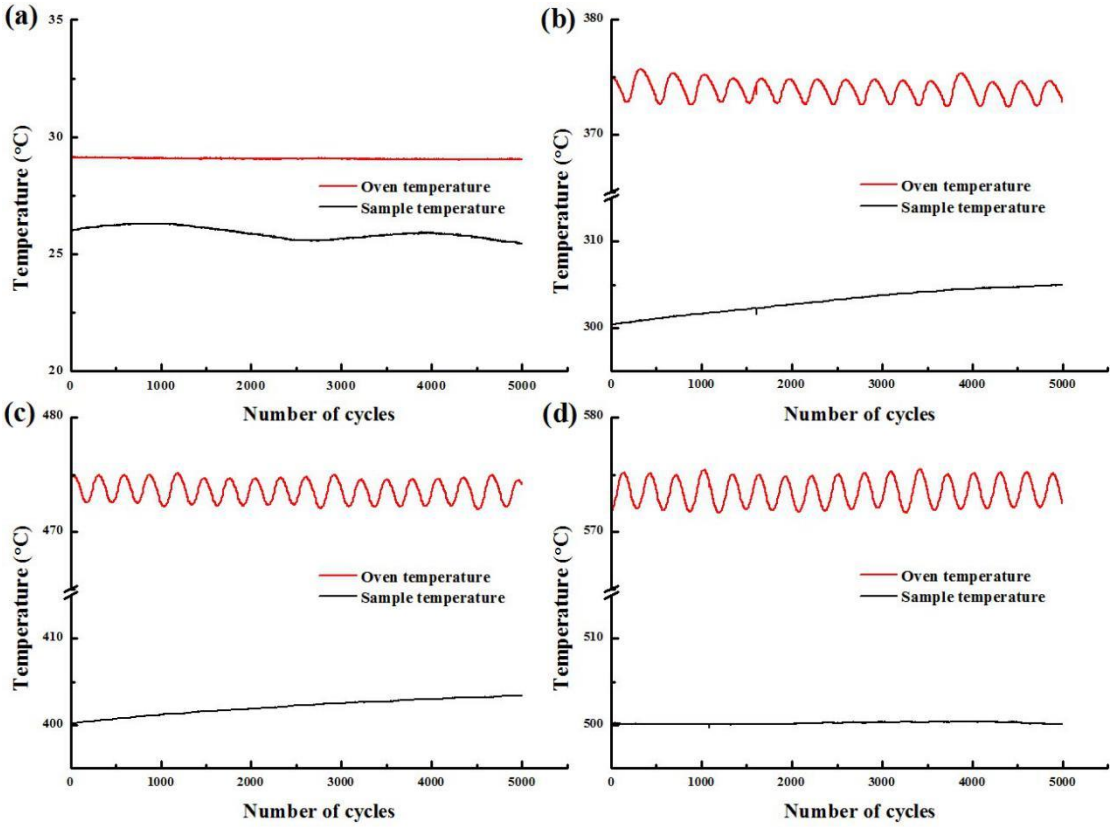
(a)
Temperature (°C)
Number of cycles
Oven temperature
Sample temperature
(b)
Temperature (°C)
Number of cycles
Oven temperature
Sample temperature
(c)
Temperature (°C)
Number of cycles
Oven temperature
Sample temperature
(d)
Temperature (°C)
Number of cycles
Oven temperature
Sample temperature

Fig. 4

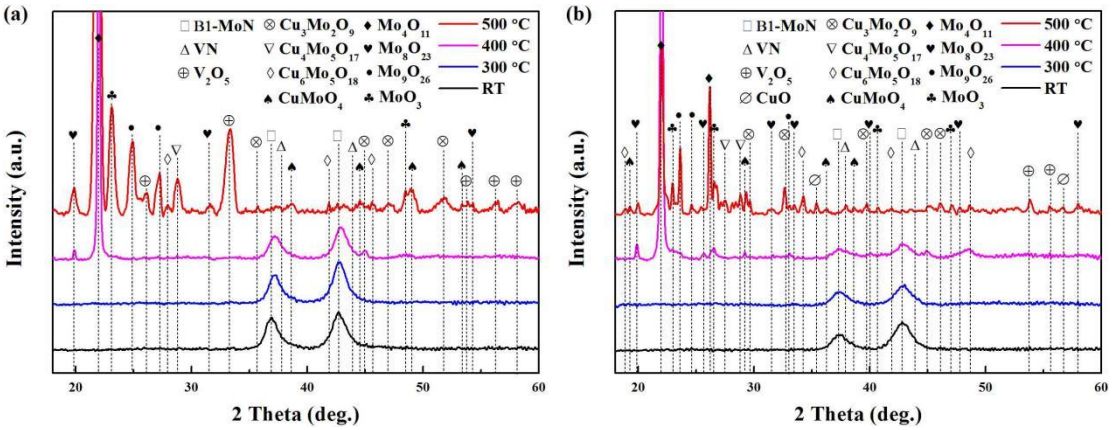
(a)
(b)
Intensity (a.u.)
2 Theta (deg.)
B1-MoN
VN
V_2O_5
$Cu_3Mo_2O_9$
$Cu_4Mo_5O_{17}$
$Cu_6Mo_5O_{18}$
$CuMoO_4$
Mo_4O_{11}
Mo_8O_{23}
Mo_9O_{26}
MoO_3
CuO
500 °C
400 °C
300 °C
RT

Fig. 5

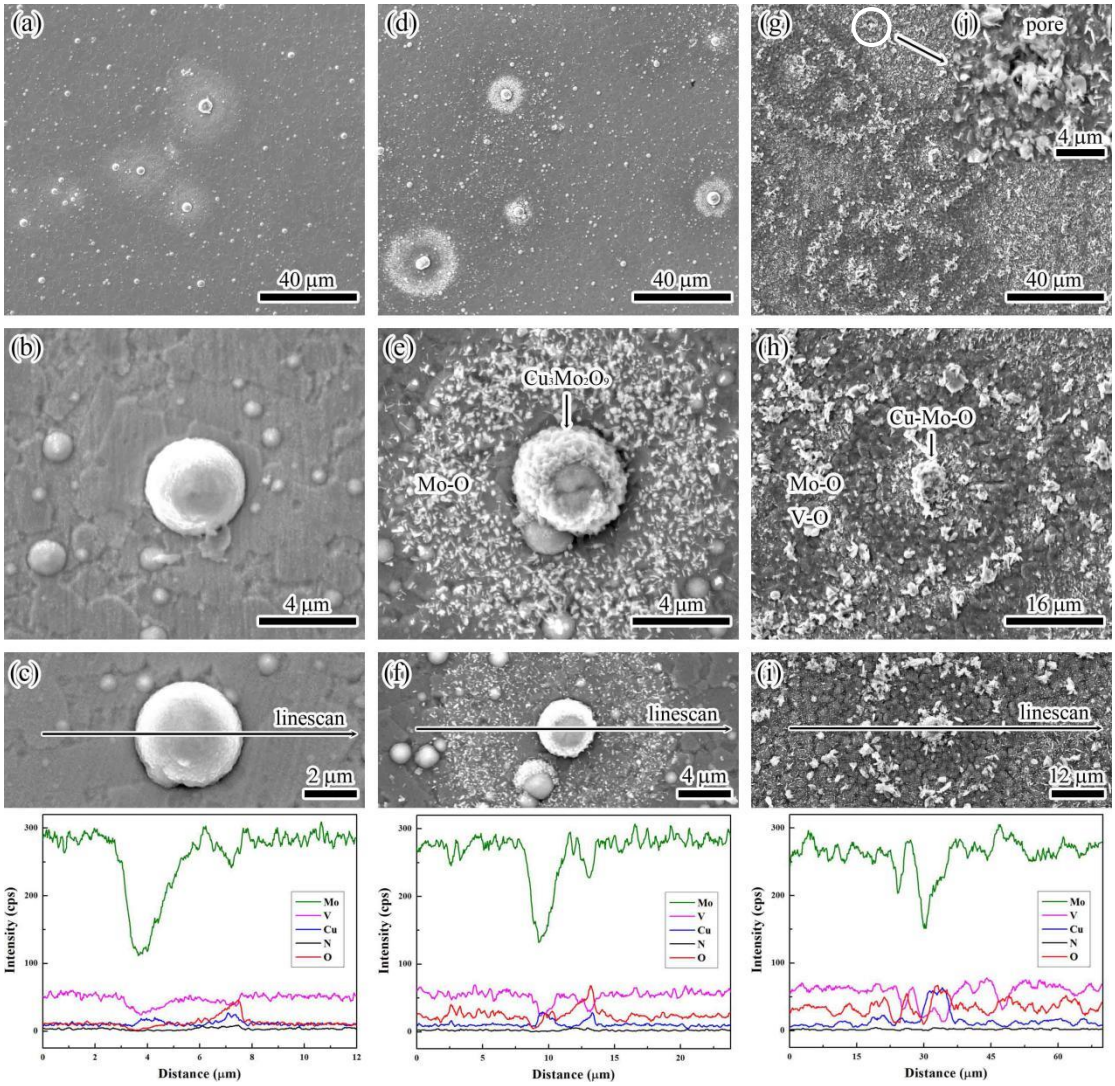
(a)
40 μm
(d)
40 μm
(g)
(j)
pore
4 μm
40 μm
(b)
4 μm
(e)
Cu3Mo2O9
Mo-O
4 μm
(h)
Cu-Mo-O
Mo-O
V-O
16 μm
(c)
linescan
2 μm
(f)
linescan
4 μm
(i)
linescan
12 μm
Intensity (cps)
Distance (μm)
Mo
V
Cu
N
O

Fig. 6

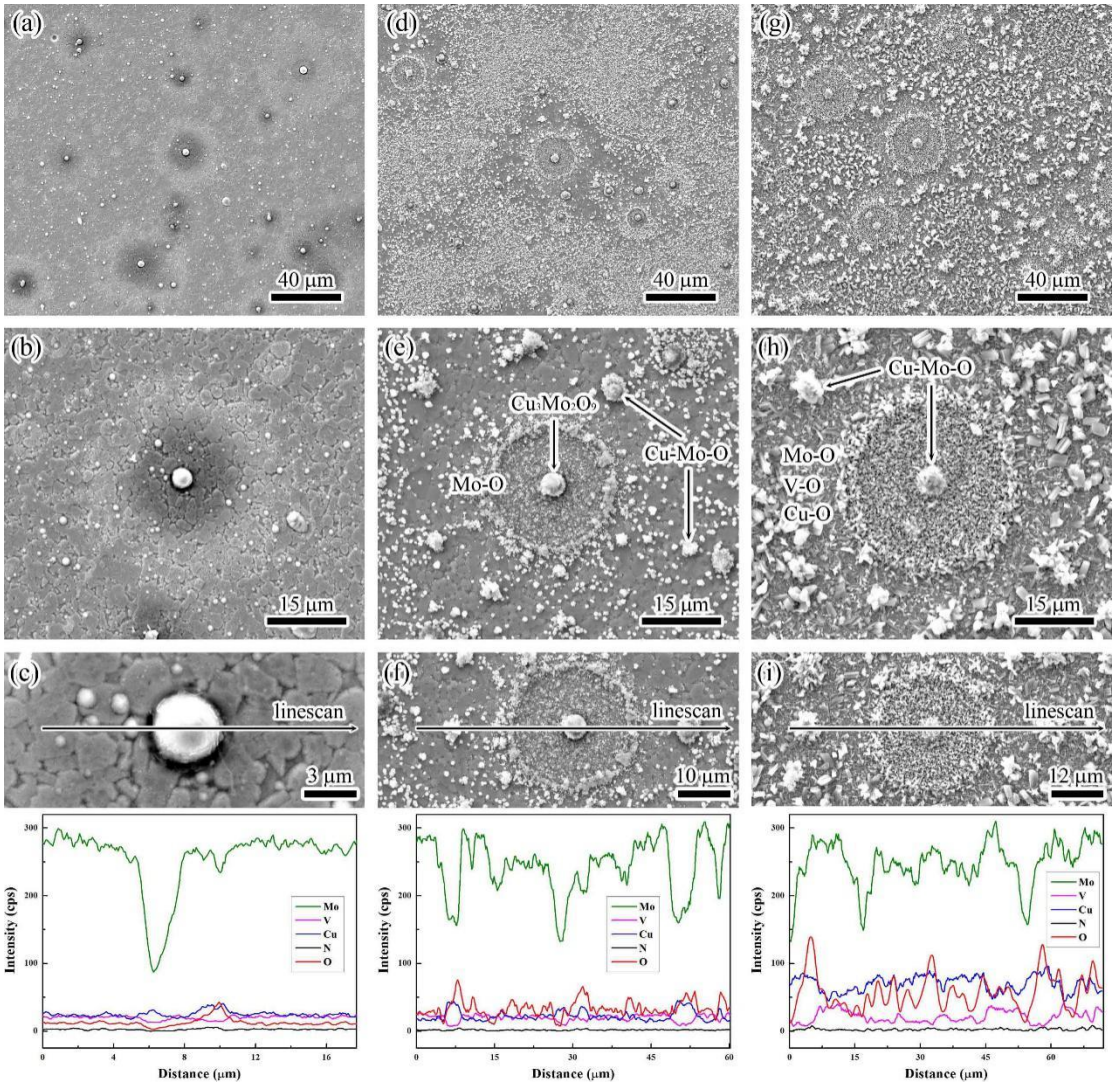
(a)
40 μm
(d)
40 μm
(g)
40 μm
(b)
15 μm
(c)
Cu3Mo2O9
Cu-Mo-O
Mo-O
15 μm
(h)
Cu-Mo-O
Mo-O
V-O
Cu-O
15 μm
(c)
linescan
3 μm
(f)
linescan
10 μm
(i)
linescan
12 μm
Intensity (cps)
Distance (μm)
Mo
V
Cu
N
O

Fig. 7

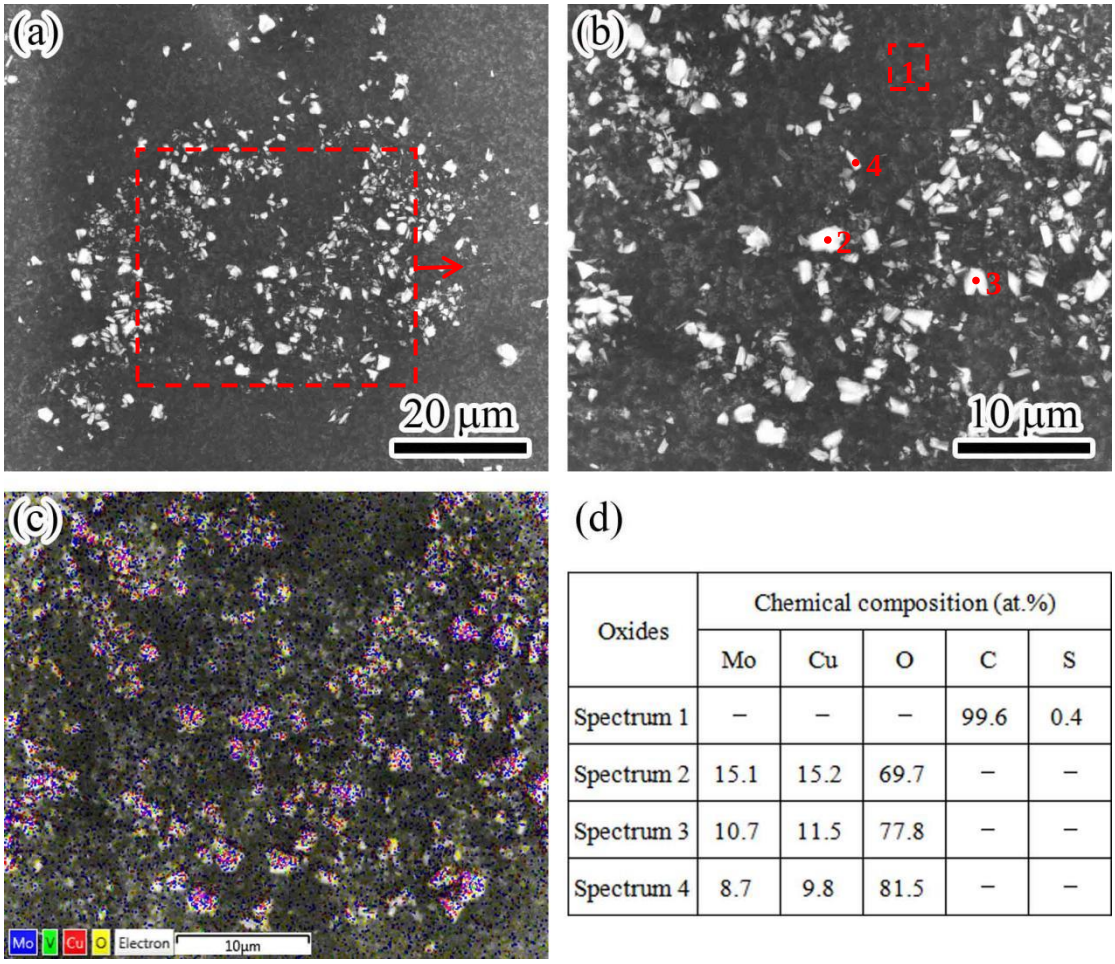

(d)

Oxides	Chemical composition (at.%)				
	Mo	Cu	O	C	S
Spectrum 1	–	–	–	99.6	0.4
Spectrum 2	15.1	15.2	69.7	–	–
Spectrum 3	10.7	11.5	77.8	–	–
Spectrum 4	8.7	9.8	81.5	–	–

Fig. 8

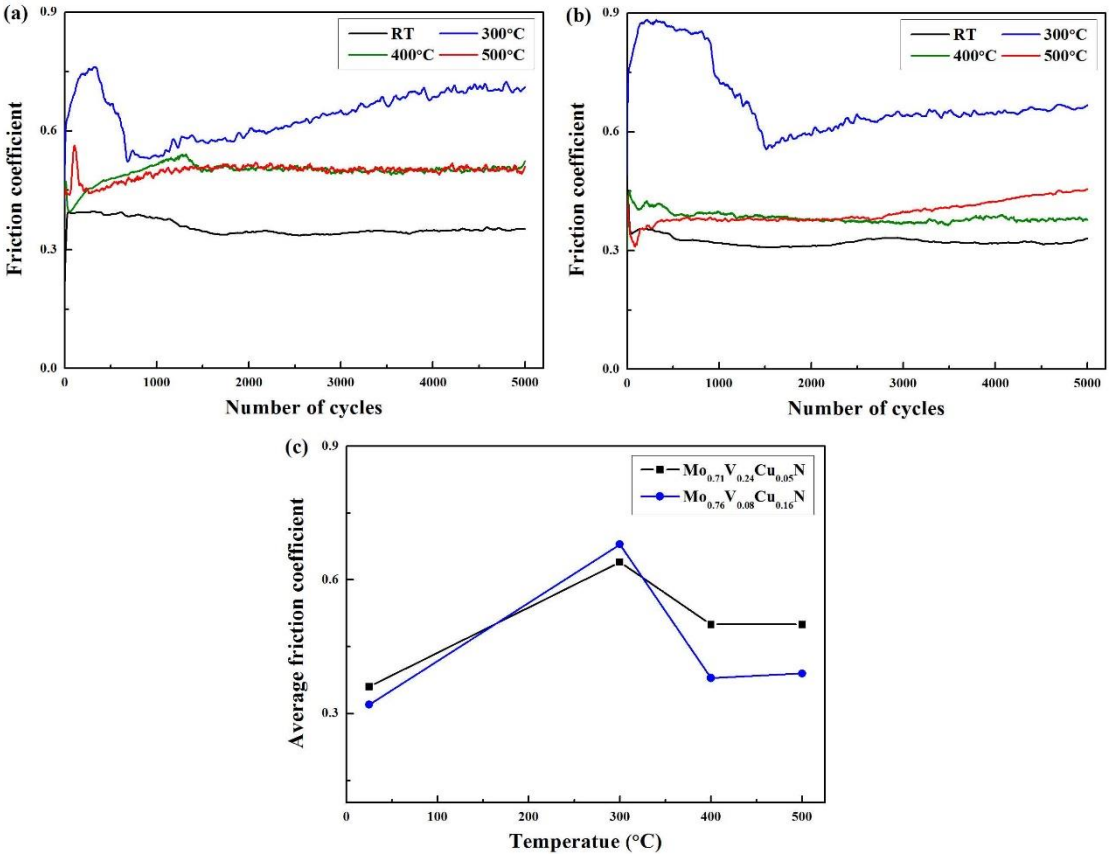
(a)
Friction coefficient
Number of cycles
RT
300°C
400°C
500°C
(b)
Friction coefficient
Number of cycles
RT
300°C
400°C
500°C
(c)
Average friction coefficient
Temperatue (°C)
Mo0.71V0.24Cu0.05N
Mo0.76V0.08Cu0.16N

Fig. 9

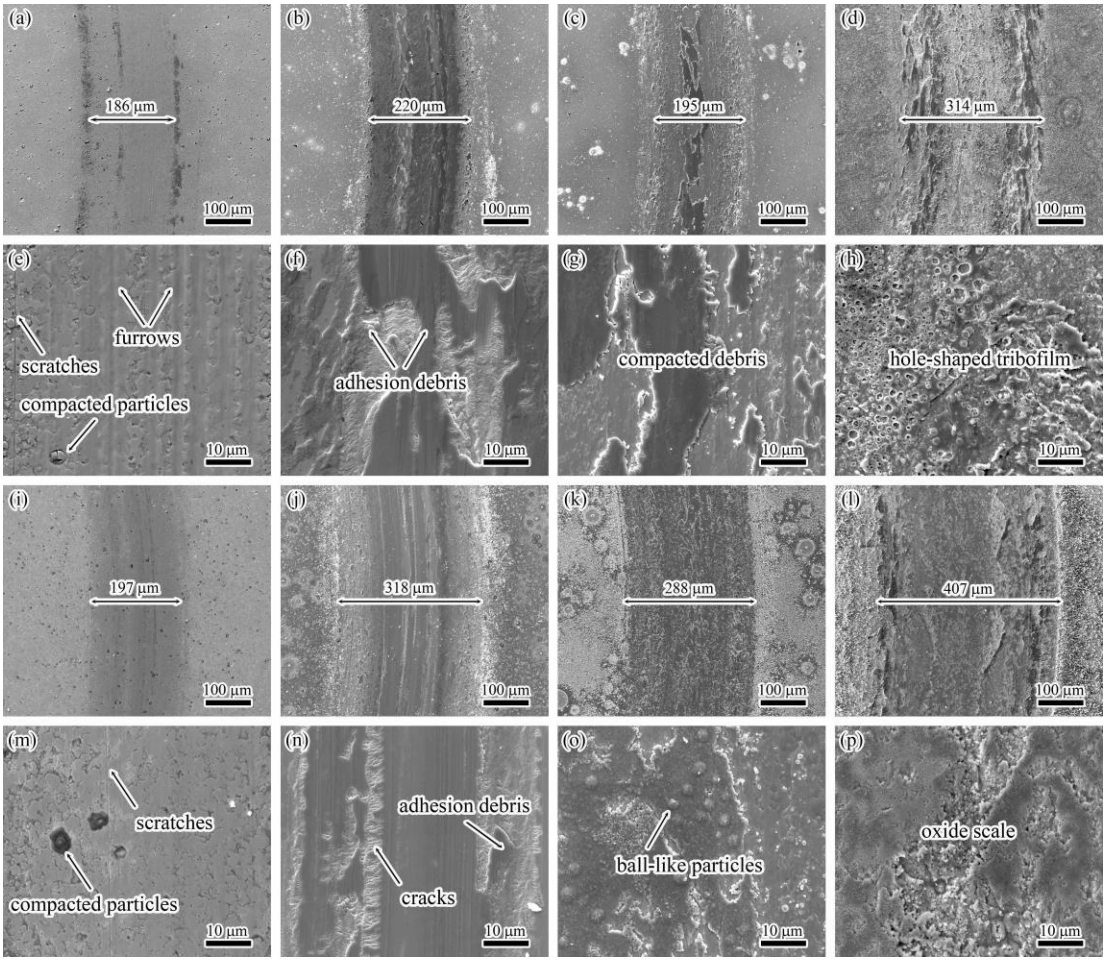
(a)
186 μm
100 μm
(b)
220 μm
100 μm
(c)
195 μm
100 μm
(d)
314 μm
100 μm
(e)
furrows
scratches
compacted particles
10 μm
(f)
adhesion debris
10 μm
(g)
compacted debris
10 μm
(h)
hole-shaped tribofilm
10 μm
(i)
197 μm
100 μm
(j)
318 μm
100 μm
(k)
288 μm
100 μm
(l)
407 μm
100 μm
(m)
scratches
compacted particles
10 μm
(n)
adhesion debris
cracks
10 μm
(o)
ball-like particles
10 μm
(p)
oxide scale
10 μm

Fig. 10

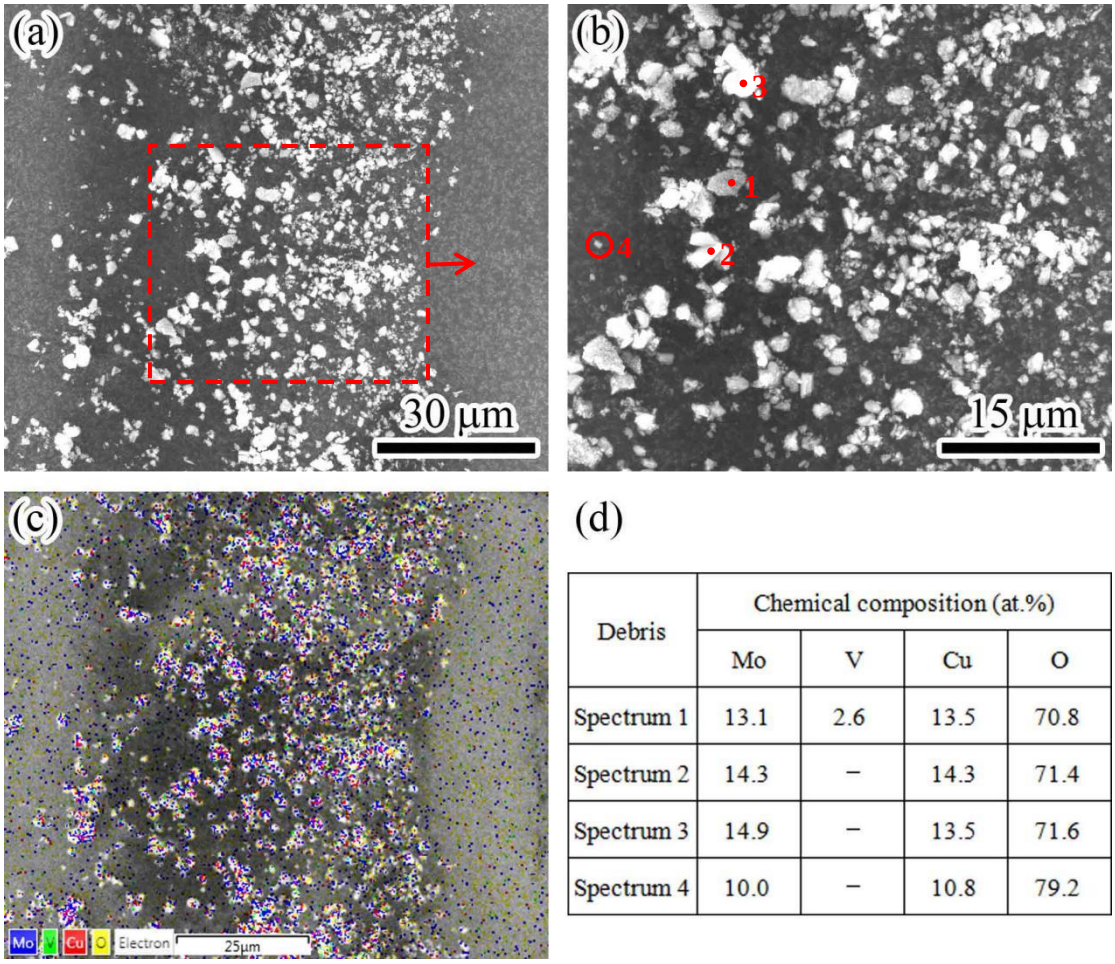

(d)

Debris	Chemical composition (at.%)			
	Mo	V	Cu	O
Spectrum 1	13.1	2.6	13.5	70.8
Spectrum 2	14.3	–	14.3	71.4
Spectrum 3	14.9	–	13.5	71.6
Spectrum 4	10.0	–	10.8	79.2

Fig. 11

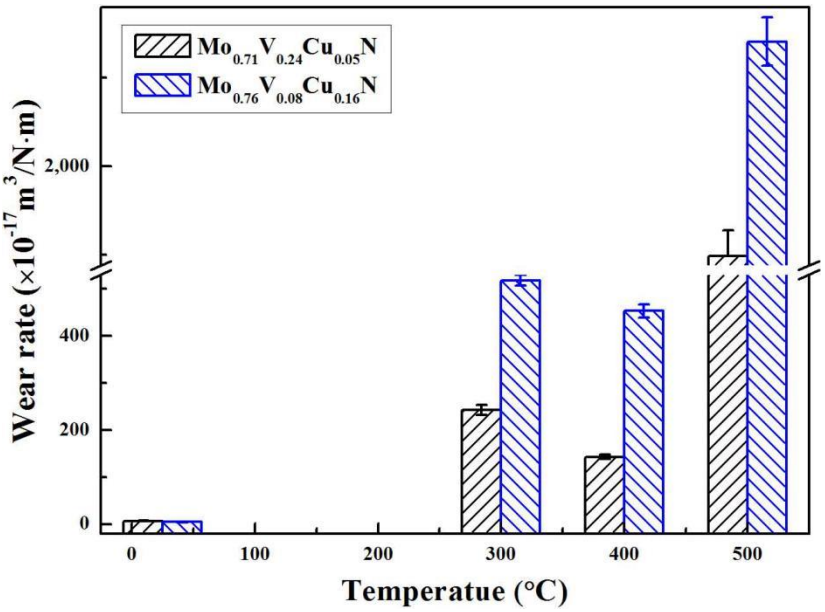
Mo0.71V0.24Cu0.05N
Mo0.76V0.08Cu0.16N
Wear rate (×10-17m3/N·m)
2,000
400
200
0
0
100
200
300
400
500
Temperatue (°C)

Fig. 12